Available online at www.sciencedirect.com
SCIENCE DIRECT®
Thin Solid Films 429 (2003) 201–210
thin solid films
www.elsevier.com/locate/tsf

Fracture toughness, adhesion and mechanical properties of low-*K* dielectric thin films measured by nanoindentation

Alex A. Volinsky[a,*], Joseph B. Vella[a], William W. Gerberich[b]

[a]*Motorola, Digital DNA™ Labs, Process and Materials Characterization Laboratory, Tempe, AZ 85284, USA*
[b]*University of Minnesota, Department of Chemical Engineering and Materials Science, Minneapolis, MN 55455, USA*

Received 3 February 2003; received in revised form 10 February 2003; accepted 14 February 2003

Abstract

The semiconductor industry is gradually moving from well-established Al/SiO_2 technology to the new Cu/low-*k* interconnects, which brings a challenge in terms of poor thermal and/or mechanical properties of low-*K* dielectric films. Extensive nanoindentation studies have been undertaken on organo-silicate glass (OSG) low-*K* films to explore their mechanical and fracture properties. A cube corner indentation method was used to measure the fracture toughness of the OSG films, which ranges from 0.01 to 0.05 $MPa \cdot m^{1/2}$. Film fracture was also observed during superlayer indentation adhesion testing. Interfacial cracks kinked into the film itself, indicating competition between adhesive and cohesive failure mechanisms. Given that the crack propagates through the low-*K*, critical stress intensities on the order of 0.05 $MPa \cdot m^{1/2}$ are estimated. This is also consistent with the upper bound calculations of 0.06 $MPa \cdot m^{1/2}$, based on spontaneous film fracture at a critical film thickness of 3 μm due to tensile residual film stress relief.

Keywords: Low-*k* dielectrics; Adhesion; Fracture toughness; Mechanical properties; Nanoindentation

1. Introduction

In order to meet the next generation device requirements, the transition from well-established Al/SiO_2 technology to new Cu/low-*k* interconnect structures is challenging, since a number of integration and reliability issues are introduced. For the new Cu/low-*K* technology reduction in the interline dimensions necessitate a reduction in the dielectric constant of traditional TEOS (tetraethyl-*ortho*-silicate) interlayer dielectric (ILD) ($k \sim 4.1$). As air has a dielectric constant of unity, one logical solution to reducing the dielectric constant of the ILD without changing the chemical composition is to introduce pores into the film. However, introducing these pores in a controlled manner with a narrow pore size distribution requires more than simply reducing TEOS density. For the CVD deposited organo-silicate glass (OSG) this problem is solved by introducing terminal methyl groups ($-CH_3$) that interrupt the Si–O network and create nano-pores, each on the order of the volume of a methyl group. However, these inclusions compromise the mechanical stability of silica, increasing the probability of mechanical failure due to a decreased concentration of Si–O bonds as well as an increased propensity for pore and density non-uniformity. Fig. 1 shows a state-of-the-art Cu six-layer interconnect structure from Motorola where the interline dielectric has been chemically removed to expose all six interconnect layers.

One challenge lies in generating a low-*k* film that can withstand chemical mechanical polishing (CMP) without fracturing or delaminating. Researchers have been putting considerable emphasis on determining hardness or Young's modulus threshold that corresponds with a material's ability to endure CMP and wire bonding processes [1–3]. In early studies at Sematech, there appeared to be a correlation between elastic modulus and the films' ability to withstand chemical–mechanical polishing. However, because these films' mechanical properties are intimately linked with their porosity,

*Corresponding author. Tel.: +1-480-413-3092; fax: +1-480-413-2656.
E-mail address: alex.volinsky@motorola.com (A.A. Volinsky).

0040-6090/03/$ - see front matter © 2003 Elsevier Science B.V. All rights reserved.
doi:10.1016/S0040-6090(03)00406-1

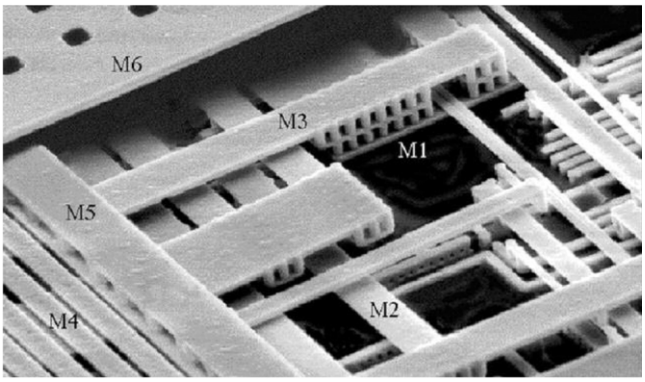

Fig. 1. Motorola copper 6-layer metallization (SEM image courtesy of Hai Nguyen, APRDL, Motorola).

trends in hardness often correspond to trends in modulus. Correlation with CMP failure can be just as easily made with the film hardness.

Fig. 2 shows the relationship of modulus and hardness that stems from the variation in porosity of a group of silicate films. There remains considerable ambiguity on how to model the mechanical properties of porous materials, utilizing foam theory [4], percolation theory [5], and finite element methods [6]; however, work in this area is ongoing [7]. Studies at Motorola [8] have indicated that CMP survivability it is not a simple factor of modulus, hardness, adhesion or toughness, but more likely a combination of all of these properties, and that developing methods to characterize each of them is therefore critical.

A viable low-*k* material candidate must be compatible with modern semiconductor processes such as etching, stripping, cleaning, damascene lithography, device packaging processes, and CMP [1,9]. The device reliability depends on many factors including the ability of the material to withstand intrinsic device stresses, the materials adhesion to its neighboring structures, and the materials ability to withstand the thermal and mechanical stresses of packaging. Typically, a multilevel IC device experiences high shear stresses during the CMP process, therefore any flaws at the interfaces or in the low-*k* film itself can lead to long-term reliability problems. Mechanical properties of thin films often differ from those of the bulk materials. This can be partially explained by the nanostructure of thin films and the fact that these films are attached to a substrate. Due to typically high yield strengths, thin films can support very high residual stresses. This residual stress can be relieved later during processing or in the actual device operation through plastic deformation, thin film fracture, or interfacial delamination. To mitigate these effects detailed reliability and compatibility tests are required to integrate new low-*k* dielectric materials and Cu interconnects.

Nanoindentation is a versatile technique for measuring films mechanical properties [10]. Thin film mechanical properties can be measured by tensile testing of free-standing films [11] and by the microbeam cantilever deflection technique [12–14], the easiest way is by means of nanoindentation, since no special sample preparation is required and tests can be performed quickly and inexpensively. Both elastic modulus and hardness can be readily extracted directly from the nanoindentation curve [10,15–17]. Since the depth resolution is on the order of nanometers, it is possible to indent even very thin (<100 nm) films. Indentation has also been used to measure thin film adhesion [18–23], where the mechanical energy release rate, or practical work of adhesion is calculated based on the size of delamination that can be generated by high load (200–800 mN) indentation.

Indentation techniques have also been used to measure fracture toughness. When a sharp tip such as Vickers, Berkovich, or a cube corner diamond is indented into bulk brittle materials, radial cracking can occur after a critical load has been reached. Typically, the sharper cube corner diamond tip is used because of the greater stress concentrations that it creates below the tip, which may induce fracture at lower critical loads. In the case of thin films, lower critical loads are necessary to minimize the inevitable substrate influence on the film fracture process. This method allows one to calculate fracture toughness based on the maximum indentation load and the crack length [24–26]. The analysis is complicated in the case of thin film radial fracture because of the halfpenny crack shape perturbation by the substrate, film densification, and residual stresses in

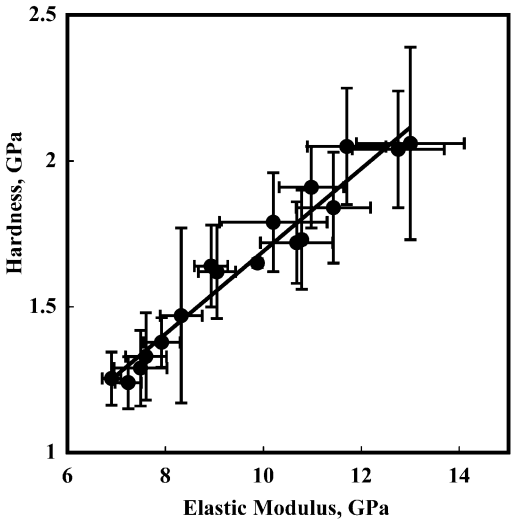

Fig. 2. Linear plot of representative silicate (OSG) low-*K* dielectric films hardness vs. modulus, demonstrating the interrelated mechanical properties of these films that stem largely from their porosity.

the film. However, current studies have yielded promising developments in this area.

2. Experiment

Several test structures have been constructed to test OSG low-*k* dielectric films mechanical properties. For the elastic modulus, hardness and fracture toughness measurements OSG films of different thicknesses ranging from 50 nm to 2.5 μm were deposited on oxidized Si wafers (with a 50 nm sputtered TaN glue layer) using a precursor CVD process. These structures are shown in Fig. 3a. For the adhesion measurements a 1-μm-thick compressive (1 GPa) TiW was sputter deposited on top of all test structures. For some of the samples a 900-nm-thick Cu layer was deposited on top of the low-*k* films to simulate real interconnect structures for CMP and determine at which interface failure would most likely occur. A schematic of the adhesion test structure cross-section is shown in Fig. 3b,c.

3. Elastic modulus and hardness

Elastic modulus and hardness measurements were carried out using a NanoIndenter XP dynamic contact module. Frequency and tip displacement modulated continuous stiffness measurements were made at a frequency of 75 Hz and an oscillation amplitude of 1 nm. Typical hardness and modulus data for a 2-μm-thick film as a function of indentation depth are shown in Fig. 4.

Elastic modulus and hardness of different low-*k* materials from different vendors were previously measured using nanoindentation [7,8], in addition to the mechanical properties measurements carried out in this study. Presently, it is not well understood whether the increase in hardness and modulus at low depths is an effect of tip adhesion, oxide damage of the low-*k* film, or an intrinsic indentation size effect [27]. It is important to note that many low-*k* films exhibit viscoelastic and viscoplastic (creep) behavior, which significantly complicates the measurement of their mechanical properties, which appear strain rate and tip oscillation frequency-dependent when measured by nanoindentation. Progress

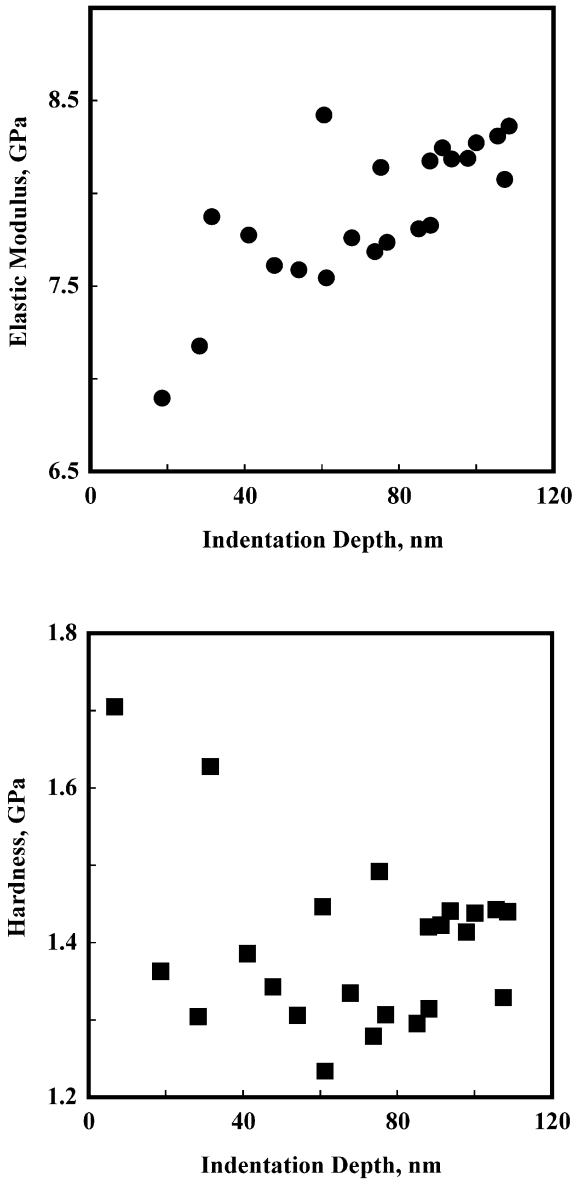

Fig. 4. Elastic modulus and hardness of a 2-μm-thick low-*K* dielectric film as a function of indentation depth.

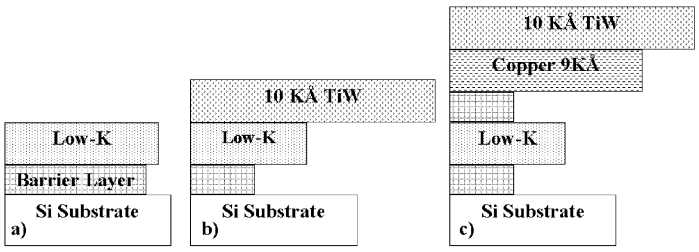

Fig. 3. Schematic of a low-*K* dielectric test structure cross-sections: (a) samples for modulus and hardness measurements; (b) samples for adhesion measurements; and (c) samples with Cu layer.

has been made in techniques utilizing spherical indentation to measure these time-dependent properties. However, the use of blunt indentation tips often precludes the use of very thin films because of the inability to localize the plastic zone underneath the tip.

Silica-based porous low-*k* films in this study have an average elastic modulus of 7 GPa and relatively high hardness of 1.3 GPa. Along with the Young's modulus and hardness, adhesion and fracture toughness are important properties to measure for low-*k* films. With low modulus to hardness ratios of these low-*k* materials and their lack of plasticity, low fracture toughness should be expected simply due to the fact that these materials are more brittle, and there is almost no plasticity at the crack tip that would normally increase fracture toughness. Fig. 2 shows almost linear relationship between elastic modulus and hardness for a range of different low-*k* materials examined outside of the current study, which can be partially explained by the nanoporous structure of these materials [7].

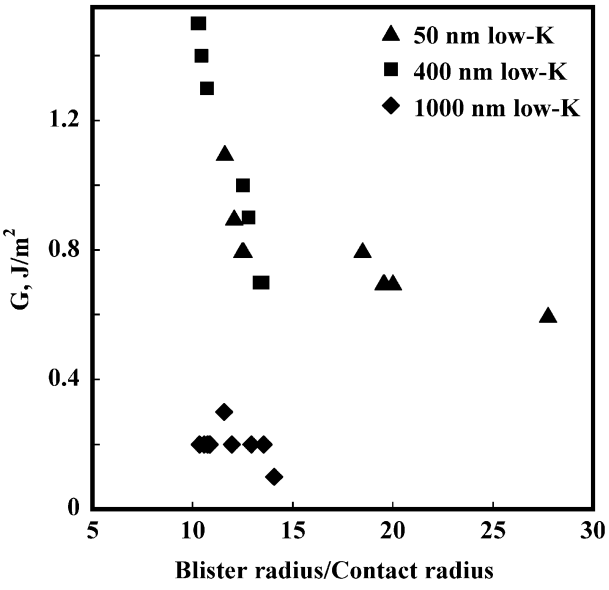

Fig. 5. Low-*K* dielectric films adhesion as a function of the blister radius to the indenter tip contact radius ratio.

4. Adhesion and fracture characterization

Beyond measuring the mechanical properties, significant advances have been made recently in measuring the adhesion strength of thin films using nanoindentaiton. Adhesion of low-*k* dielectric films was measured by means of the superlayer indentation technique [20–23]. Most well-adhered or low modulus thin films cannot be delaminated by means of regular indentation: most ductile films tend to deform plastically around the indenter by forming pileup and consequently will relieve the indentation stress rather than transferring it to the interfacial crack tip. To prevent these problems a high modulus hard superlayer, capable of supporting and storing large amounts of elastic energy is deposited on top of the film of interest. Upon indentation a delamination blister forms around the indent, and its area is used to calculate the strain energy release rate (practical work of adhesion).

Typically for a given thickness thin film adhesion varies approximately 20–30% [23]. Fig. 5 shows a large variation in the low-*k* film adhesion, from 0.2 to 1.5 J/m^2. Several delamination blisters have been cross-sectioned using Focused Ion Beam (FIB), and it was found that the low-*k* fracture is generally cohesive (Fig. 6). Since low-*K* dielectrics have low elastic modulus and are relatively thin, it is possible to apply superlayer indentation analysis [20,23] for estimating the resistance to cohesive crack propagation. With the high hardness to modulus ratios one may expect low fracture toughness of these materials. What is really measured in this case is the fracture toughness of the low-*K* film itself, and the high spread in the mechanical energy release rate values is explained by *R*-curve behavior.

Fracture characterization presented in Figs. 6–8 shows the crack path in the test structures. The only low-*K* film that exhibited signs of interfacial failure is a 1-μm-thick film with extremely low adhesion value of 0.2 J/m^2. Fig. 7 represents interfacial or near-interfacial failure in the low-*K* dielectric with the crack kink from the low-*K*/substrate to the low-*K*/TiW interface. While measuring low-*K* film adhesion other researchers have also observed cracks in the low-*K* close to the interface [33]. Typically, the analysis for assessing the mechanical energy release rate would still be valid due to the fact that the low-*K* layer is very thin and the low-*K* elastic modulus is much lower compared to other layers. For any adhesion test the results should not be taken blindly, and determining the crack path should be a part of adhesion assessments and fracture characterization.

For the structures with a Cu layer (Fig. 3c), low-*K* cohesive failure was also observed, implying that the films stack interfacial toughness exceeds the low-*K* film toughness. Given that the crack propagates through the low-*K* during these tests and based on resultant mechanical energy release rate calculations [20,22,23], and film elastic modulus measurements, film toughness up to 0.05 MPa·m$^{1/2}$ can be estimated. Using an average value of 7 GPa for the low-*K* modulus (Fig. 4), this corresponds to a strain energy release rate of 0.36 J/m^2. This is intermediate to the lower values of the superlayer test results of 0.2 to 0.8 J/m^2 in Fig. 5. This also agrees with the film toughness values calculated from the critical film cracking thickness based on the knowledge of the residual stress shown in the next section.

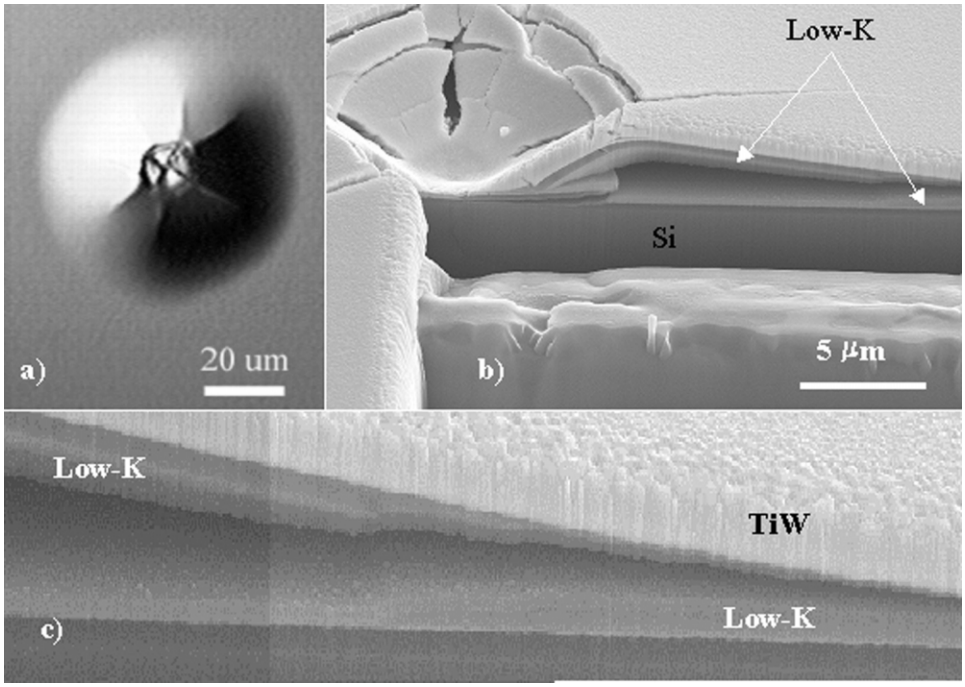

Fig. 6. (a) Nomarski contrast optical image of the TiW/400 nm low-*K* dielectric blister; (b) SEM micrograph of the FIB cross-section of the blister in (a); and (c) SEM image showing low-*K* dielectric cohesive failure.

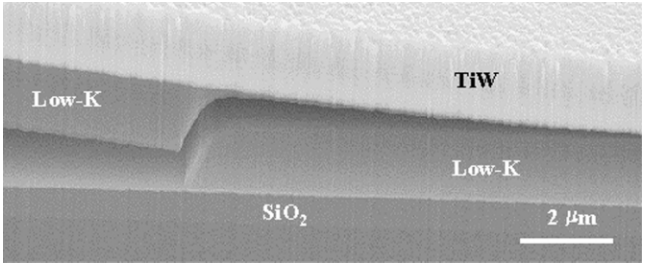

Fig. 7. Interfacial failure in a 1 μm low-*K* dielectric film showing the crack kink.

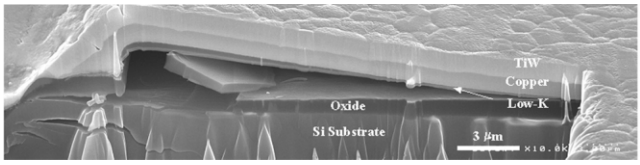

Fig. 8. FIB cross-section of the indentation-induced blister delamination in the Cu/low-*K* dielectric structure showing cohesive low-*K* dielectric failure.

Several samples have exhibited phone cord delamination upon deposition of a highly compressed TiW superlayer. Typical examples are shown in Fig. 9. Given the superlayer thickness of 1 μm and the residual stress of 1 GPa, and the elastic modulus of 275 GPa, the amount of stored elastic energy that has been released

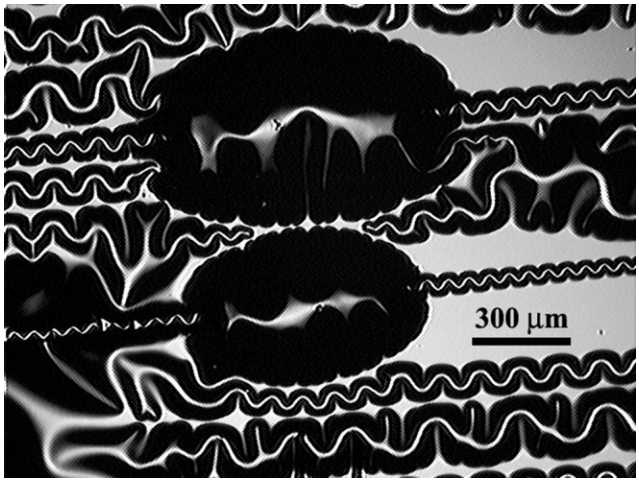

Fig. 9. Phone cord buckling delamination pattern of the TiW/low-*K* dielectric structures.

during the delamination process can be estimated following Hutchinson and Suo [34]:

$$G = Z\frac{(1-\nu_f^2)\sigma_R^2 h}{E_f} \quad (1)$$

where σ_R is the residual stress, h is the film thickness, and E_f is the film elastic modulus, and Z ranges from 0.5 to 4 [34], depending on the sample geometry and the residual stress sign. Ignoring the effect of the low-

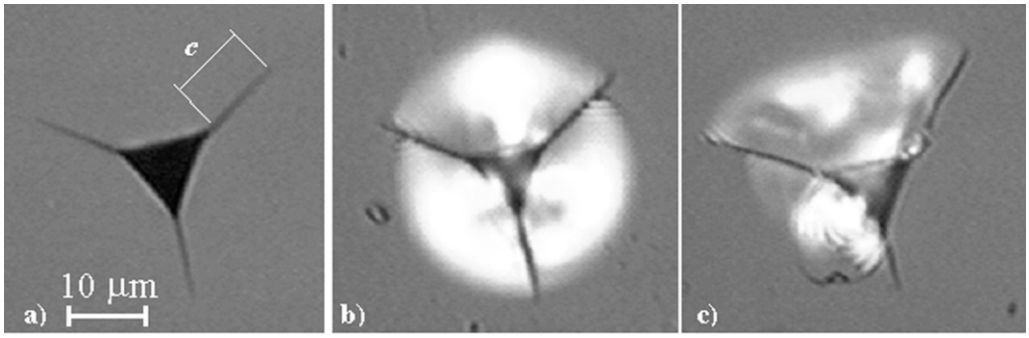

Fig. 10. Optical micrographs of cube-corner indentation-induced fracture in fused silica: (a) radial cracks; (b) radial and symmetric sub-surface cracks; and (c) radial and asymmetric sub-surface cracks.

modulus low-K film, one can estimate 1.86 J/m^2 for the amount of energy per unit area released, which is an upper bound to the low-K adhesion/toughness values ranging from 0.5 to 1.5 J/m^2 (Fig. 5). A simple analysis like this can provide realistic upper estimates of the thin film adhesion/toughness.

5. Low-K dielectic film fracture toughness

After realizing that in most cases there is a competition between the interfacial adhesion and film toughness, and that cohesive fracture is observed in the case of low-K films, we made attempts to measure thin film toughness more accurately using nanoindentation.

Fracture toughness of a bulk brittle material can be calculated within 40% accuracy based on the maximum indentation depth, P_{max} and the crack length, c (Fig. 10a) [25,26]:

$$K_C = \alpha\left(\frac{E}{H}\right)^{1/2}\left(\frac{P_{max}}{c^{3/2}}\right) \quad (2)$$

where α is an empirical constant which depends on the geometry of the indenter, and is 0.0319 for a cube corner indenter geometry [25], E is the elastic modulus, and H is the mean hardness. This expression should not be directly applied in the case of a thin film, since typically the crack shape is no longer halfpenny shape, as assumed in the original analysis. Although, technically speaking, any type of pyramid can induce radial cracks, it was shown that the cube-corner indenter provides a lower cracking threshold in terms of the maximum indentation load [26].

Fig. 10 shows three different scenarios one may observe using pyramid indentation. Fig. 10a is the desired configuration for radial cracks emanating from the corners of an indent. Due to the high shear stresses induced by the indenter pyramid edges, subsurface delamination cracks were also observed for some indents (Fig. 10b,c). Lawn and Wilshaw [35] provide a detailed review of the indentation-induced cracking in bulk brittle materials. For the fracture toughness calculations only 'perfect' indents as in Fig. 10a were used. On average, we calculate 0.5 MPa·m$^{1/2}$ for the fracture toughness of fused quartz, which is lower compared to the literature value of 0.75 MPa·m$^{1/2}$ [36]. Although low, this is within the typical 40% error of the test.

Compared to the indentation-induced fracture in bulk fused quartz, low-K films show similar cracking patterns (Fig. 11). For the fracture toughness measurements purposes we only consider 'perfect' indents that result

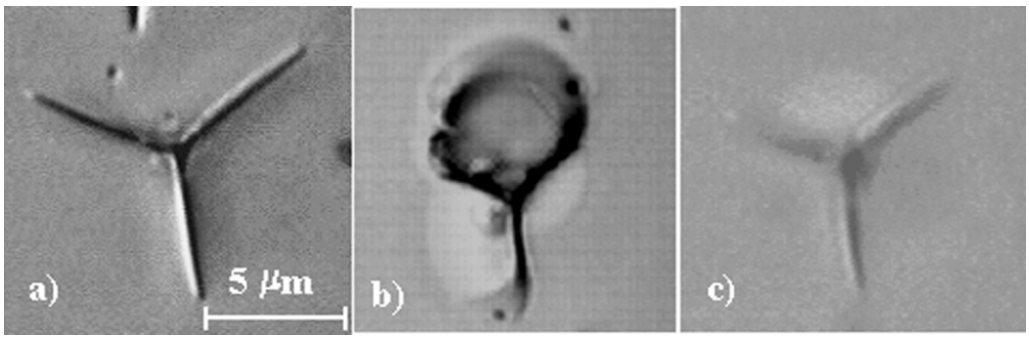

Fig. 11. Optical micrographs of cube-corner indentation-induced fracture in low-K dielectric films: (a) 2-μm-thick film; (b) radial and delamination cracks in a 1-μm-thick film; and (c) 1-μm-thick film.

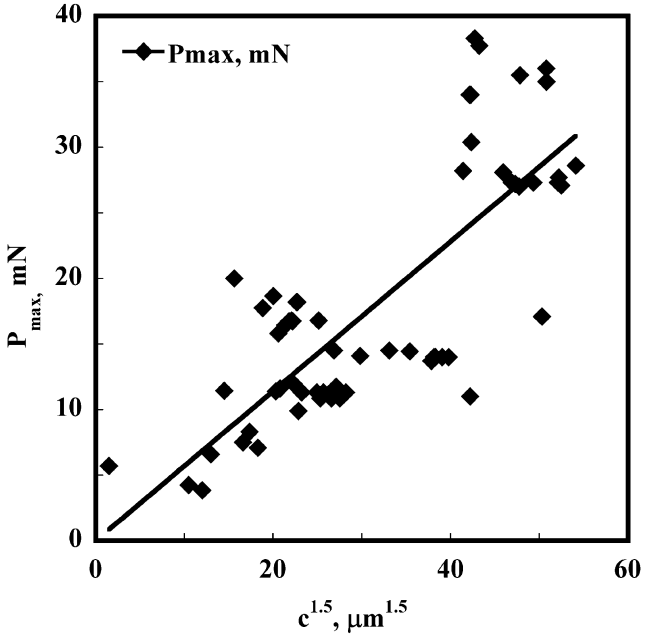

Fig. 12. Maximum indentation load, P_{max} as a function of $c^{3/2}$.

with radial through-thickness cracks (Fig. 11a,c), and not interfacial delamination (Fig. 11b) cracks.

We realize that Eq. (2) should not be directly applied for the case of a thin film fracture since the crack shape is not halfpenny. Still, a plot of the maximum indentation load as a function of the crack length to the $3/2$ power demonstrates a fairly linear relationship (Fig. 12). A to a first order approximation, Eq. (2) was used to estimate the low-K films fracture toughness. Using this method we estimate low-K dielectric films fracture toughness to range from 0.01 to 0.05 MPa·m$^{1/2}$.

An additional method utilized for measuring toughness involves a lateral scratch, which causes a tangential stress at the trailing edge of the scribe. This has been utilized by both Ostartage et al. [28] and Hoehn et al. [29], noting that

$$K_C = 2\sigma_{\theta\theta}\left(\frac{c}{\pi}\right)^{1/2}\cdot\sin^{-1}\left(\frac{a}{c}\right) \tag{3}$$

where a is the contact radius and c is the half crack. Since a/c is almost always less than $1/2$, $\sin^{-1}(x)\sim x$ and with $\sigma_{\theta\theta}=P_{max}/\pi a^2$, one finds that Eq. (3) reduces to:

$$K_C \approx \frac{2P_{max}}{\pi^{3/2}}\cdot\frac{1}{ac^{1/2}} \approx \text{const}\cdot\left(\frac{P_{max}}{c^{3/2}}\right) \tag{4}$$

with the latter approximation coming if $c/a\sim$constant. This then is the same as Eq. (2), since $(E/H)^{1/2}$ is nearly constant in Fig. 1. However, both Eqs. (2) and (4) have inherent composite yield strength, modulus and strain energy release rate built into a laminate system needing detailed analysis.

One of the ways to more accurately solve this problem would be to use FEM calculations of the stress field around the indenter, taking into account low-K film thickness and residual stress. As cracks in the low-K are more tunnel-like, and do not propagate into the substrate, an analysis by Beuth may be appropriate [30]. In general, fracture toughness of a thin film can either increase or decrease with the film thickness. For example, thicker W films on steel are tougher, but W(C) film toughness decreases with the film thickness due to the limited crack tip plasticity [31]. Low-K films are brittle

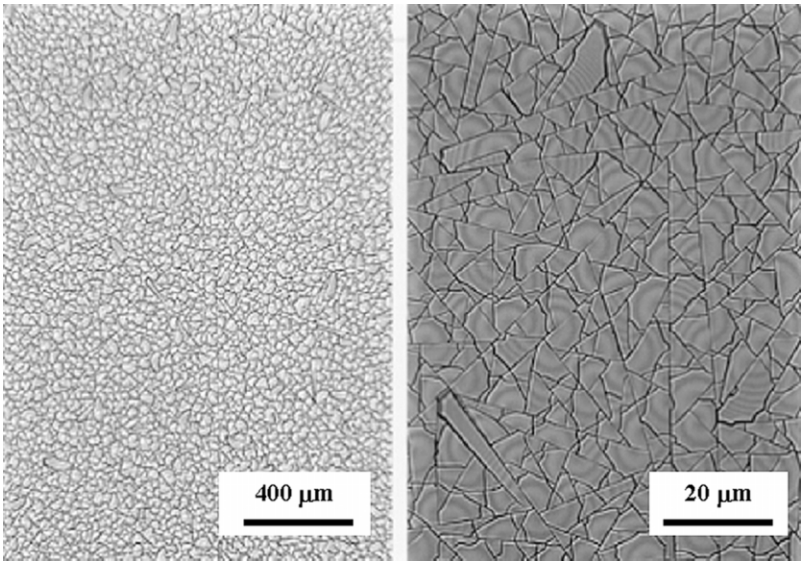

Fig. 13. Plan views of a cracked 3-μm-thick low-K dielectric film.

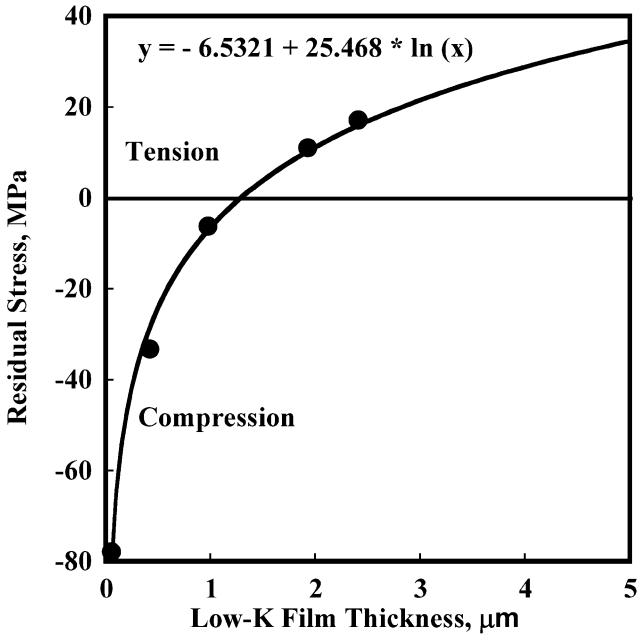

Fig. 14. Low-*K* dielectric stack residual stress as a function of the film thickness along with the logarithmic function fit.

and porous so one should not expect toughness to increase with the film thickness. In fact, we observe low-*K* film fracture just because of the residual stress relief (Fig. 13).

6. Low-*K* dielectric film residual stress

It is also important to consider the effect of residual stress on the low-*K* fracture process. In the present study it was found that at approximately 3 μm thickness low-*K* films form through-thickness cracks due to the residual stress relief (Fig. 13). Low-*K* dielectric film stack residual stress measured using the wafer curvature technique is shown in Fig. 14 as a function of the film thickness. The residual stress can be best fit with the logarithmic function, also presented in Fig. 14.

$$\sigma_R = A + B\ln(h) \tag{5}$$

where *A* and *B* are the fitting parameters, and *h* is the film thickness.

If we consider residual stress as the only source of film failure, the strain energy release rate would be described by Eq. (1). From fracture mechanics the stress intensity in plane strain is related to the strain energy release rate as:

$$K^2(1-\nu_f^2) = GE_f \tag{6}$$

so *K* just due to the residual strain would be:

$$K = \sigma_R\sqrt{Zh} \tag{7}$$

where *Z* is described at Eq. (1). Note that the elastic modulus cancels out, so Eq. (7) remains true also for the plane stress conditions. Now we can write a failure criterion based on the knowledge of the residual stress and the film thickness:

$$K_C \le \sigma_R\sqrt{Zh} \tag{7a}$$

For a constant level of residual stress thicker films would be more susceptible to failure. Eq. (7) is similar to a definition of *K*, except here the film thickness is used instead of the flaw size, or the crack length [32]. Physically, this means that thicker films would have larger flaw size. This can be explained by higher surface roughness of thicker films, or using the Weibull statistics, where thicker films would have higher volume, thus higher probability of having larger defect through the film thickness. Taking 25 MPa tensile residual stress for a 3 μm film (Fig. 14), and $Z = 1.976$ for channel cracks [34], gives 0.06 MPa·m$^{1/2}$.

We can use the general log function for the residual stress from Eq. (5) and express *K* in terms of the residual stress as a function of the film thickness:

$$K \le |A + B\log h| \cdot (Zh)^{1/2} \tag{8}$$

Here, we use the absolute stress values due to the fact that both tensile and compressive stresses cause film fracture. The only difference between compression and tension is the failure mode (buckling vs. through-thickness channeling cracking, both of which may be accompanied by interfacial film debonding). Strictly speaking, the *Z* values are different for tensile and compressive residual stress and are given in [34]. *K* normalized by $Z^{1/2}$ from Eq. (8) is plotted along with the measured low-*K* fracture toughness in Fig. 15. Converting the average K_{IC} values of 0.02 to 0.03 MPa·m$^{1/2}$ to the strain energy release rates gives 0.06 to 0.13 J/m^2, which is just slightly less than the delamination fracture resistance of the low-*K* films in Fig. 5. This demonstrates in general that it is the toughness of the low-*K* material itself, and not the adhesion that is controlling the fracture process. At approximately 1 μm film thickness there is a transition from compressive to tensile residual stress, so the amount of stored elastic energy in the film is minimal. Measured film toughness for the 1-μm-thick films are much higher than the calculated values due to the residual stress, while there is agreement for the largest thickness values. Additional energy (from nanoindentation, CMP, etc.) is required to fracture the thinner films. On the other hand, for the thicker films calculated

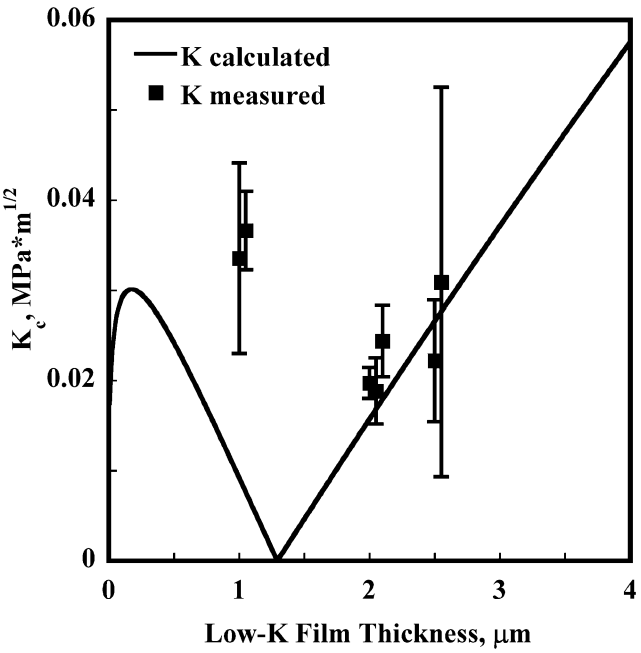

Fig. 15. Measured low-*K* dielectric film fracture toughness compared to the normalized *K* values due only to the film residual stress [Eq. (8)].

residual stress fracture toughness values are comparable to the measured ones, so film fracture just due to the residual stress relief is quite possible, as observed in Fig. 13. The measured low-*K* fracture toughness values range from 0.01 to 0.05 MPa·m$^{1/2}$, which is lower than the low-*K* interfacial adhesion (0.037 to 0.1 MPa·m$^{1/2}$).

7. Conclusions

In this study, we consider the nanoindentation technique for measuring elastic modulus, hardness, adhesion and fracture toughness of low-*K* dielectric thin films. For the films studied hardness scales with elastic modulus, and fracture toughness is extremely low through the film thickness and at the interface. We were able to measure low-*K* film toughness using both the superlayer and the cube corner indentation tests. Maximum measured fracture toughness is quite low, approaching 0.05 MPa·m$^{1/2}$. This appears to be consistent with the results from both indentation tests and calculations based on film self-fracture due to the residual stress relief for thicker films.

Low-*K* films studied are far from being ideal for product integration due to poor mechanical performance. Mechanical properties should to be optimized in terms of improved fracture resistance. Nanoindentation techniques were successfully applied for measuring a variety of low-*K* dielectric films mechanical properties, from presently almost routine elastic modulus to more challenging fracture toughness measurements. A lower bound failure criterion based on the thin film residual stress is proposed.

Acknowledgments

Authors would like to acknowledge the support of the APRDL low-*K* group: Burt Fowler, Kurt Junker, Cindy Goldberg, Nicole Grove. From PMCL: Indira Adhihetty, Ginger Edwards, Bruce Xie, Marti Erikson, and Susan Urbas. David Joy from the University of Tennessee for valuable discussions.

References

[1] Y.L. Wang, C. Liu, S.T. Chang, M.S. Tsai, M.S. Tsai, M.S. Fang, W.T. Tseng, Thin Solid Films 308–309 (1997) 550.
[2] E. Hartmannsgruber, G. Zwicker, K. Beekmann, Microelectron. Eng. 50 (2000) 53.
[3] H. Yano, Y. Matsui, G. Minamihaba, N. Kawahashi, M. Hattori, Mater. Res. Soc. Proc. 671 (2001) M2.4.
[4] E.O. Shaffer II, K.E. Howard, M.E. Mills, P.H. Townsend III, Mater. Res. Soc. Proc. 612 (2000) D1.1.
[5] J. Kovacik, J. Mater. Sci. Lett. 18 (13) (1999) 1007.
[6] A.P. Roberts, E.J. Garboczi, J. Am. Ceram. Soc. 83 (12) (2000) 3041.
[7] J.B. Vella, Q. Xie, N.V. Edwards, J. Kulik, K. Junker, Mater. Res. Soc. Proc. 695 (2001) L6.25.
[8] I.S. Adhihetty, J.B. Vella, A.A. Volinsky, C. Goldberg, W.W. Gerberich, Proceedings of the 10th International Congress on Fracture, Honolulu, USA, December 2–6, 2001, Nanoscale Problems Symposium. Organized by W.W. Gerberich, R.H. Dauskardt, K. Tanaka.
[9] C.L. Borst, V. Korthuis, G.B. Shinn, J.D. Luttmer, R.J. Gutmann, W.N. Gill, Thin Solid Films 385 (2000) 281.
[10] W.W. Gerberich, W. Yu, D. Kramer, A. Strojny, D. Bahr, E. Lilleodden, J. Nelson, J. Mater. Res. 13 (2) (1998) 421.
[11] D.T. Read, J.W. Dally, J. Mater. Res. 8 (7) (1993) 1542.
[12] T.P. Weihs, S. Hong, J.C. Bravman, W.D. Nix, J. Mater. Res. 3 (5) (1998) 931.
[13] S.P. Baker, W.D. Nix, J. Mater. Res. 9 (12) (1994) 3131.
[14] S.P. Baker, W.D. Nix, J. Mater. Res. 9 (12) (1994) 3145.
[15] M. Doerner, W.D. Nix, J. Mater. Res. 1 (1986) 601.
[16] G.M. Pharr, W.C. Oliver, F. Brotzen, J. Mater. Res. 7 (3) (1992) 613.
[17] W.C Oliver, G.M. Pharr, J. Mater. Res. 7 (1992) 1564.
[18] D.B. Marshall, A.G. Evans, J. Appl. Phys. 56 (1984) 2632.
[19] J.J. Vlassak, M.D. Drory, W.D. Nix, J. Mater. Res. 12 (7) (1997) 1900.
[20] M.D. Kriese, W.W. Gerberich, J. Mater. Res. 14 (7) (1999) 3007.
[21] M.D Kriese, W.W. Gerberich, N.R. Moody, J. Mater. Res. 14 (7) (1999) 3019.
[22] A.A. Volinsky, N.I. Tymiak, M.D. Kriese, W.W. Gerberich, J.W. Hutchinson, Mater. Res. Soc. Symp. Proc. 539 (1999) 277.
[23] A.A. Volinsky, N.R. Moody, W.W. Gerberich, Acta Mater. 50/3 (2002) 441.
[24] G.R. Antis, P. Chantikul, B.R. Lawn, D.B. Marshall, J. Am. Ceram. Soc. 64 (9) (1981) 533.
[25] G.M. Pharr, D.S. Harding, W.C. Oliver, in: M. Nastasi, Don M. Parkin, H. Gleiter (Eds.), Oliver Mechanical Properties and

Deformation Behavior of Materials Having Ultra-Fine Microstructures, Kluwer Academic Press, 1993, p. 449.
[26] D.S. Harding, W.C. Oliver, G.M. Pharr, Mater. Res. Soc. Symp. Proc. 356 (1995) 663.
[27] J.C. Grunlan., X. Xia, D. Rowenhost, W.W. Gerberich, Rev. Sci. Instrum. 72 (6) (2001) 1523.
[28] C.P. Ostartage, P.C. Churalambides, A.G. Evans, Acta Mater. 37 (7) (1989) 2077.
[29] J.W. Hoehn, S.K. Venkataraman, H. Huang, W.W. Gerberich, Mater. Sci. Eng. A 192/193 (1995) 306.
[30] J.L. Beuth Jr., Int. J. Solids Struct. 29 (13) (1992) 1657.
[31] E. Harry, A. Rouzaud, M. Ignat, P. Juliet, Thin Solid Films 332 (1998) 195.
[32] D.B. Marshall, B.R. Lawn, A.G. Evans, J. Am. Ceram. Soc. 65 (11) (1982) 561.
[33] R.H. Dauskardt, Adhesion and mechanical reliability of new low-*K* materials for interconnect structures, Mechanics and Materials Summer Conference, San Diego, USA, June 27–29, 2001 MMC2001 Book of Abstracts, 2001, p. 109.
[34] J. Hutchinson, Z. Suo, Adv. Appl. Mech. 29 (1992) 63.
[35] B. Lawn, R. Winslaw, J. Mater. Sci. 10 (1975) 1049.
[36] M.W. Barsoum, Fundamentals of Ceramics, McGraw-Hill, 1997.